



This discussion paper is/has been under review for the journal Geoscientific Model Development (GMD). Please refer to the corresponding final paper in GMD if available.

Mapping of satellite Earth observations using moving window block kriging

J. M. Tadić, X. Qiu, V. Yadav, and A. M. Michalak

Department of Global Ecology, Carnegie Institution for Science, Stanford, CA 94305, USA

Received: 24 July 2014 – Accepted: 28 July 2014 – Published: 8 August 2014

Correspondence to: J. M. Tadić (jotadic@lycos.com)

Published by Copernicus Publications on behalf of the European Geosciences Union.

GMDD

7, 5381–5405, 2014

**Mapping of satellite
Earth observations
using moving
window block kriging**

J. M. Tadić et al.

Title Page

Abstract

Introduction

Conclusions

References

Tables

Figures



Back

Close

Full Screen / Esc

Printer-friendly Version

Interactive Discussion



Abstract

Global gridded maps (a.k.a. Level 3 products) of Earth system properties observed by satellites are central to understanding the spatiotemporal variability of these properties. They also typically serve either as inputs into biogeochemical models, or as independent data for evaluating such models. Spatial binning is a common method for generating contiguous maps, but this approach results in a loss of information, especially when the measurement noise is low relative to the degree of spatiotemporal variability. Such “binned” fields typically also lack a quantitative measure of uncertainty.

Geostatistical mapping has previously been shown to make higher spatiotemporal resolution maps possible, and also provides a measure of the uncertainty associated with the gridded products. This study proposes a flexible moving window block kriging method that can be used as a tool for creating high spatiotemporal resolution maps from satellite data. It relies only on the assumption that the observed physical quantity exhibits spatial correlation that can be inferred from the observations. The method has several innovations relative to previously applied methods: (1) it provides flexibility in the spatial resolution of the contiguous maps (2) it is applicable for physical quantities with varying spatiotemporal coverage (i.e., density of measurements) by utilizing a more general and versatile data sampling approach, and (3) it provides rigorous assessments of the uncertainty associated with the gridded products. The method is demonstrated by creating Level 3 products from observations of column-integrated carbon dioxide (XCO_2) from the GOSAT satellite, and solar induced fluorescence (SIF) from the GOME-2 instrument.

1 Introduction

Satellite measurements of an Earth surface and atmospheric quantities have enormous benefits for Earth system science due to their global coverage and near real-time availability. They provide key constraints for developing models representing our

GMDD

7, 5381–5405, 2014

Mapping of satellite Earth observations using moving window block kriging

J. M. Tadić et al.

Title Page

Abstract

Introduction

Conclusions

References

Tables

Figures



Back

Close

Full Screen / Esc

Printer-friendly Version

Interactive Discussion



satellite measurements, and (3) provide rigorous assessments of the uncertainty associated with the contiguous maps.

2 Methods

The proposed approach builds on the work of Hammerling et al. (2012a, b), with the goal of increasing the applicability and the flexibility of the nonstationary local kriging approach presented therein. The main innovations are twofold. The first is to allow flexibility in the spatial support of the estimates (i.e. the spatial resolution at which the mapping is conducted). The second is to provide a general approach for subsampling available observations in a manner that (i) captures the local correlation structure in the vicinity of each estimation grid cell and (ii) makes the statistical mapping approach computationally feasible in the case of applications with a very large number of observations.

The mapping proceeds in three steps for each grid cell and each estimation time on a regular grid, in order to create a contiguous map of the satellite observations. These steps are outlined in the subsections below, and include subsampling of the observations, characterization of the local spatial covariance structure, and interpolation at the desired spatial resolution. In Sect. 3, the new mapping approach is applied to two prototypical examples of satellite observations, namely observations of column-integrated concentration of atmospheric CO₂ concentrations (XCO₂) and observations of surface solar induced fluorescence (SIF), measured by the GOSAT satellite, and by the GOME instrument, respectively.

2.1 Subsampling of observations

The goal of the subsampling strategy is to preferentially sample observations in the vicinity of a given estimation grid cell, such that both the characterization of the local spatial covariance structure, and the ultimate mapped estimate and its associated

Mapping of satellite Earth observations using moving window block kriging

J. M. Tadić et al.

Title Page

Abstract

Introduction

Conclusions

References

Tables

Figures



Back

Close

Full Screen / Esc

Printer-friendly Version

Interactive Discussion



window. The window size was based in part on expected scales of variability in the satellite observations. The updated approach presented here reduces the number of user-selected parameters, and explicitly provides a mechanism for ensuring the computational feasibility of mapping in the case of very large datasets, such as the SIF example examined here.

2.2 Characterization of spatial covariance

The characterization of the local covariance structure of the observations around each estimation grid cell, based on the subsampled observations, proceeds as described in Hammerling et al. (2012a, Sect. 2.1), except that (1) all possible pairs of observations are included in the formulation of the raw variogram, and the nugget-effect variance, representative of the retrieval/measurement errors, is not spatially uniform. The reader is referred to that earlier publication for additional details.

Briefly, for each estimation grid cell, a raw variogram is calculated based on the subsampled observations:

$$\gamma(h) = \frac{1}{2} [y(x_i) - y(x_j)]^2 \quad (3)$$

where γ is the raw variogram value for a given pair of observations $y(x_i)$ and $y(x_j)$, and h is the great circle distance between the locations (x_i and x_j) of these observations, as defined in Eq. (2).

A parametric function, the theoretical variogram, is fitted to the raw variogram using non-linear least squares. For the prototypical applications presented here, an exponential variogram function with a nugget effect was used, because it yields a valid covariance function on a sphere (Huang et al., 2011), provided a good match to the known physical characteristics of the observations, and fit the observed variability well:

$$\gamma(h) = \begin{cases} 0, & \text{for } h = 0 \\ \sigma^2(1 - \exp(-\frac{h}{\tau}) + \sigma_{\text{nug}}^2, & \text{for } h > 0 \end{cases} \quad (4)$$

Mapping of satellite Earth observations using moving window block kriging

J. M. Tadić et al.

Title Page

Abstract

Introduction

Conclusions

References

Tables

Figures

◀

▶

◀

▶

Back

Close

Full Screen / Esc

Printer-friendly Version

Interactive Discussion



where σ^2 and l are the variance and correlation length of the quantity being mapped, and σ_{nug}^2 is the nugget variance, typically representative of measurement and retrieval errors in the case of satellite observations. The nugget component can be either prescribed (as in the XCO₂ example in Sect. 3) or estimated (as in the SIF example in Sect. 3), depending on the availability of information about measurement and retrieval errors.

The variogram parameters can be used to define a corresponding local spatial covariance structure for the mapped quantity (XCO₂ or SIF, in the prototypical examples presented here). For the variogram function in Eq. (4) this becomes:

$$q(h) = \sigma^2 \exp\left(-\frac{h}{l}\right) \quad (5)$$

The nugget effect is correspondingly used to define the covariance structure of the measurement and retrieval errors:

$$R(h) = \begin{cases} \sigma_{\text{nug}}^2, & \text{for } h = 0 \\ 0, & \text{for } h > 0 \end{cases} \quad (6)$$

2.3 Mapping using moving window block kriging

Ordinary kriging, a minimum variance linear unbiased mapping method for spatial data, was used in Hammerling et al. (2012a, b) to create contiguous maps of XCO₂. In this approach, the spatial support (i.e. footprint) of the estimates corresponds to that of the observations. Although the mapping can be performed at any spatial interval (e.g. once per 1° × 1° grid cell), the estimates remain representative of the variability at the scale of the observations.

Here, we instead use block kriging (e.g. Webster, 2000), an approach that yields estimates that represent an average within a specified area. This makes it possible to disassociate the native footprint of the observations from the resolution of the mapped

Mapping of satellite Earth observations using moving window block kriging

J. M. Tadić et al.

Title Page

Abstract

Introduction

Conclusions

References

Tables

Figures

⏪

⏩

◀

▶

Back

Close

Full Screen / Esc

Printer-friendly Version

Interactive Discussion



Mapping of satellite Earth observations using moving window block kriging

J. M. Tadić et al.

Title Page

Abstract

Introduction

Conclusions

References

Tables

Figures

◀

▶

◀

▶

Back

Close

Full Screen / Esc

Printer-friendly Version

Interactive Discussion



product, thereby making it possible to create contiguous maps at any desired spatial resolution equivalent to or greater than the size of the observation footprints. As with moving window ordinary kriging, block kriging provides an optimal estimate of the quantity being mapped (XCO₂ and SIF, in the prototypical examples presented here) for each estimation location, based on the subsampled observations (Sect. 2.1) and the local covariance structure (Sect. 2.2), together with a rigorous assessment of the uncertainty associated with the estimate.

The linear system of equations that is solved to obtain the N weights λ assigned to the subsampled observations for a given estimation grid cell is:

$$\begin{bmatrix} \mathbf{Q} + \mathbf{R} & \mathbf{1} \\ \mathbf{1}^T & 0 \end{bmatrix} \begin{bmatrix} \lambda \\ -\nu \end{bmatrix} = \begin{bmatrix} \mathbf{q}_A \\ 1 \end{bmatrix} \quad (7)$$

where \mathbf{Q} is a $N \times N$ covariance matrix among the N observations with individual entries as defined in Eq. (5), \mathbf{R} is an $N \times N$ diagonal measurement and retrieval error covariance matrix among the N observations as defined in Eq. (6), $\mathbf{1}$ is an $N \times 1$ unity vector, T denotes the vector transpose operation, and \mathbf{q}_A is an $N \times 1$ vector of the spatial covariances between the estimation grid cell and the N observation locations, defined as:

$$q_{A,i} = \frac{1}{n} \sum_{j=1}^n q(h_{i,j}) \quad (8)$$

where $q_{A,i}$ is the covariance between the grid cell and observation i , and $q(h_{i,j})$ is defined as in Eq. (5) based on the distance $h_{i,j}$ between observation i and n regularly-spaced locations within the grid cell. In general, the larger the n the better the representation of the area (i.e. grid cell) to observation covariance. For practical purposes, in the applications presented here, n is defined based on the relative footprint of the observations compared to that of the estimation grid cells.

The system in Eq. (7) is solved for λ and the Lagrange multiplier ν . These parameters are then used to define the estimate (\hat{z}) and estimation uncertainty variance (σ_z^2) for

compared to those presented for an equivalent period in Hammerling (2012b, Auxiliary Figs. 2 and 3), with methodological differences as described in Sect. 2, and representative of the estimated XCO₂ at the native resolution of sounding footprints (nadir footprint ~ 10.5 km diameter) with estimates at 1° × 1.25° intervals.

Results show that, because of the information content of the sparse observations, the estimated fields (Fig. 2a and c) are similar at native and 1° × 1°, but that estimating directly at the coarser 1° × 1° resolution yields lower uncertainties as observations become more informative for spatially-averaged quantities (Fig. 3). The largest reduction in uncertainty occurs in the high northern latitudes, an area identified in a previous study as one of the most weakly constrained regions (Hammerling et al., 2012b).

3.2 Global land solar-induced fluorescence fields observed by GOME-2

A series of recent studies has demonstrated the potential use of satellite observations of solar-induced fluorescence (SIF) for understanding and quantifying photosynthetic CO₂ uptake at large scales, using data from the GOSAT satellite (e.g., Joiner et al., 2011, 2012; Frankenberg et al., 2011, 2012; Guanter et al., 2012; Lee et al., 2013), the SCIAMACHY (SCanning Imaging Absorption spectroMeter for Atmospheric CHartographY) instrument on board ENVISAT (e.g., Joiner et al., 2012), the GOME-2 (The Global Ozone Monitoring Experiment-2) instrument on board METOP-A (e.g., Joiner et al., 2013), and the Orbiting Carbon Observatory (OCO-2) (e.g., Frankenberg et al., 2014). Satellite measurements of fluorescence can be used with land surface models to improve the representation of GPP and to understand GPP response to environmental stress (e.g., Lee et al., 2013). Among available datasets, GOME-2 provides the highest spatial and temporal density of data.

Until now, studies of SIF have relied on spatially and temporally binned average observations at monthly or coarser timescales and 1° or coarser spatial scales (e.g., Fig. 4). The coarse spatial and temporal scales were used to overcome, through the use of simple averaging, spatial gaps in observations and the relatively high uncertainties associated with individual retrievals. One of the limitations of such an approach

Mapping of satellite Earth observations using moving window block kriging

J. M. Tadić et al.

Title Page

Abstract

Introduction

Conclusions

References

Tables

Figures



Back

Close

Full Screen / Esc

Printer-friendly Version

Interactive Discussion



Mapping of satellite Earth observations using moving window block kriging

J. M. Tadić et al.

Title Page

Abstract

Introduction

Conclusions

References

Tables

Figures

⏪

⏩

◀

▶

Back

Close

Full Screen / Esc

Printer-friendly Version

Interactive Discussion



choice of optimal temporal resolution thus, in general, defines a trade-off between having sufficient observations for adequate spatial coverage, while minimizing the impact of temporal variability in the quantity being examined (Hammerling et al., 2012a). From Fig. 6 it is apparent that the presented approach makes it possible to obtain maps at temporal resolutions much higher than the monthly (or coarser) resolution of current binned products. As expected, the more abundant observations available at 6 day temporal resolution (Fig. 6d) lead to decreased estimation uncertainty compared to 1 day resolution (Fig. 6b). However, at monthly temporal resolutions (Fig. 6e and f) the temporal variability in SIF over a 31 day period increases the discrepancy among (spatially) nearby observations, leading to increased uncertainties at coarse time scales. This effect is apparent in comparing Fig. 6d and f, as uncertainty increases over, for example, eastern South America. A similar trade-off was also noted in selecting mapping timescales for XCO₂ (Hammerling et al., 2012a), and further speaks to the advantage of being able to select a mapping timescale based on scientific need and uncertainty tolerance, as is possible with the approach presented here.

4 Conclusions

In this study we propose a flexible moving window block kriging method that can be used as a tool for creating high spatiotemporal resolution maps from satellite data. The method can be applied in a standalone mode, or as a part of broader satellite data processing package. The resulting maps can also be incorporated into biogeochemical and physical models of the Earth system. The approach relies only on the assumption that the observed physical quantity exhibits spatial correlation that can be inferred from the observations. The method has several advantages over previously applied methods: (1) it allows for the creation of contiguous maps at varying spatio-temporal resolution, (2) it can be applied for creating contiguous maps for physical quantities with varying spatio-temporal coverage (aka density of measurements), (3) it provides assessments of the uncertainty of interpolated values. The approach emphasizes the

Japanese parties (NIES, JAXA, MOE) for making the GOSAT spectra available to the scientific community. We also thank Joanna Joiner (NASA/GSFC) for providing GOME-2 SIF data, and NASA Carbon Cycle Science program (NNH10DA001N) for funding the SIF research.

References

- 5 Alkhaled, A. A., Michalak, A. M., Olsen, S., Kawa, S. R., and Wang, J.-W.: A global evaluation of the regional spatial variability of column integrated CO₂ distributions, *J. Geophys. Res.-Atmos.*, 113, D20303, doi:10.1029/2007JD009693, 2008.
- Atkinson, P. M. and Curran, P. J.: Defining an optimal size of support for remote sensing investigations, *IEEE T. Geosci. Remote*, 33, 768–776, 1995.
- 10 Baker, I. T., Berry, J. A., Lee, J., Frankenberg, C., and Denning, S.: Constraining Simulated Photosynthesis with Fluorescence Observations, American Geophysical Union, Fall Meeting 2012, abstract #B12B-02, 2012.
- Basu, S., Guerlet, S., Butz, A., Houweling, S., Hasekamp, O., Aben, I., Krummel, P., Steele, P., Langenfelds, R., Torn, M., Biraud, S., Stephens, B., Andrews, A., and Worthy, D.: Global CO₂ fluxes estimated from GOSAT retrievals of total column CO₂, *Atmos. Chem. Phys.*, 13, 8695–8717, doi:10.5194/acp-13-8695-2013, 2013.
- 15 Basu, S., Krol, M., Butz, A., Clerbaux, C., Sawa, Y., Machida, T., Matsueda, H., Frankenberg, C., Hasekamp, O. P., and Aben, I.: The seasonal variation of the CO₂ flux over Tropical Asia estimated from GOSAT, CONTRAIL, and IASI, *Geophys. Res. Lett.*, 41, 1809–1815, doi:10.1002/2013GL059105, 2014.
- 20 Braverman, A., Nguyen, H., Olsen, E., Miller, C., Cressie, N., Kratzfuss, M., Wang, R., and Michalak, A.: Geostatistical data fusion for remote sensing applications, NASA Annu. Rep., Apr. 2011, 2011 Report from the ESTO Advanced Information Systems Technology (AIST) Program, NASA, Greenbelt, MD, USA, 2011.
- 25 Chevallier, F., Palemer, P. I., Feng, L., Boesch, H., O'Dell, C. W., and Bousquet, P.: Toward robust and consistent regional CO₂ flux estimates from in situ and spaceborne measurements of atmospheric CO₂, *Geophys. Res. Lett.*, 41, 1065–1070, doi:10.1002/2013GL058772, 2014.
- Chiles, J.-P. and Delfiner, P.: *Geostatistics*, 2nd edn., Wiley, 2012.

Mapping of satellite Earth observations using moving window block kriging

J. M. Tadić et al.

Title Page

Abstract

Introduction

Conclusions

References

Tables

Figures



Back

Close

Full Screen / Esc

Printer-friendly Version

Interactive Discussion



CO₂ DAAD: <http://dge.stanford.edu/labs/michalaklab/CO2DAAD/XCO2maps.html>, last access: 23 July 2014.

Collins, J. B. and Woodcock, C. E.: Geostatistical estimation of resolution-dependent variance in remotely sensed images, *Photogramm. Eng. Rem. S.*, 65, 41–50, 1999.

Crevoisier, C., Chédin, A., Matsueda, H., Machida, T., Armante, R., and Scott, N. A.: First year of upper tropospheric integrated content of CO₂ from IASI hyperspectral infrared observations, *Atmos. Chem. Phys.*, 9, 4797–4810, doi:10.5194/acp-9-4797-2009, 2009.

Crisp, D., Fisher, B. M., O'Dell, C., Frankenberg, C., Basilio, R., Bösch, H., Brown, L. R., Castano, R., Connor, B., Deutscher, N. M., Eldering, A., Griffith, D., Gunson, M., Kuze, A., Mandrake, L., McDuffie, J., Messerschmidt, J., Miller, C. E., Morino, I., Natraj, V., Notholt, J., O'Brien, D. M., Oyafuso, F., Polonsky, I., Robinson, J., Salawitch, R., Sherlock, V., Smyth, M., Suto, H., Taylor, T. E., Thompson, D. R., Wennberg, P. O., Wunch, D., and Yung, Y. L.: The ACOS CO₂ retrieval algorithm – Part II: Global X_{CO₂} data characterization, *Atmos. Meas. Tech.*, 5, 687–707, doi:10.5194/amt-5-687-2012, 2012.

Deng, F., Jones, D. B. A., Henze, D. K., Bousseres, N., Bowman, K. W., Fisher, J. B., Nassar, R., O'Dell, C., Wunch, D., Wennberg, P. O., Kort, E. A., Wofsy, S. C., Blumenstock, T., Deutscher, N. M., Griffith, D. W. T., Hase, F., Heikkinen, P., Sherlock, V., Strong, K., Sussmann, R., and Warneke, T.: Inferring regional sources and sinks of atmospheric CO₂ from GOSAT XCO₂ data, *Atmos. Chem. Phys.*, 14, 3703–3727, doi:10.5194/acp-14-3703-2014, 2014.

Frankenberg, C., Fisher, J. B., Worden, J., Badgley, G., Saatchi, S. S., Lee, J.-E., Toon, G. C., Butz, A., Jung, M., Kuze, A., and Yokota, T.: New global observations of the terrestrial carbon cycle from GOSAT: patterns of plant fluorescence with gross primary productivity, *Geophys. Res. Lett.*, 38, L17706, doi:10.1029/2011GL048738, 2011.

Frankenberg, C., O'Dell, C., Guanter, L., and McDuffie, J.: Remote sensing of near-infrared chlorophyll fluorescence from space in scattering atmospheres: implications for its retrieval and interferences with atmospheric CO₂ retrievals, *Atmos. Meas. Tech.*, 5, 2081–2094, doi:10.5194/amt-5-2081-2012, 2012.

Frankenberg, C., O'Dell, C., Berry, J., Guanter, L., Joiner, J., Köhler, P., Pollock, R., and Taylor, T. E.: Prospects for chlorophyll fluorescence remote sensing from the Orbiting Carbon Observatory-2, *Remote Sens. Environ.*, 147, 1–12, doi:10.1016/j.rse.2014.02.007, 2014.

GOSAT Project: <http://www.gosat.nies.go.jp/eng/gosat/page5.htm>, last access: 23 July 2014.

Mapping of satellite Earth observations using moving window block kriging

J. M. Tadić et al.

Title Page

Abstract

Introduction

Conclusions

References

Tables

Figures



Back

Close

Full Screen / Esc

Printer-friendly Version

Interactive Discussion



Mapping of satellite Earth observations using moving window block kriging

J. M. Tadić et al.

Title Page

Abstract

Introduction

Conclusions

References

Tables

Figures

◀

▶

◀

▶

Back

Close

Full Screen / Esc

Printer-friendly Version

Interactive Discussion



Guanter, L., Frankenberg, C., Dudhia, A., Lewis, P. E., Gomez-Dans, J., Kuze, A., Suto, H., and Grainger, R. G.: Retrieval and global assessment of terrestrial chlorophyll fluorescence from GOSAT space measurements, *Remote Sens. Environ.*, 121, 236–251, doi:10.1016/j.rse.2012.02.006, 2012.

5 Guerlet, S., Basu, S., Butz, A., Krol, M., Hahne, P., Houweling, S., Hasekamp, O. P., and Aben, I.: Reduced carbon uptake during the 2010 Northern Hemisphere summer from GOSAT, *Geophys. Res. Lett.*, 40, 2378–2383, doi:10.1002/grl.50402, 2013.

Haas, T. C.: Lognormal and moving window methods of estimating acid deposition, *J. Am. Stat. Assoc.*, 85, 950–963, 1990.

10 Hammerling, D. M., Michalak, A. M., and Kawa, S. R.: Mapping of CO₂ at high spatiotemporal resolution using satellite observations: global distributions from OCO₂, *J. Geophys. Res.*, 117, D06306, doi:10.1029/2011JD017015, 2012a.

Hammerling, D. M., Michalak, A. M., O'Dell, C., and Kawa, S. R.: Global CO₂ distributions over land from the Greenhouse Gases Observing Satellite (GOSAT), *Geophys. Res. Lett.*, 39, L08804, doi:10.1029/2012GL051203, 2012b.

15 Harris, P., Charlton, M., and Fotheringham, A. S.: Moving window kriging with geographically weighted variograms, *SERRA*, 24, 1193–1209, 2010.

Huang, C., Zhang, H., and Robeson, S. M.: On the validity of commonly used covariance and variogram functions on the sphere, *Math. Geosci.*, 43, MR2824128, 721–733, 2011.

20 Joiner, J., Yoshida, Y., Vasilkov, A. P., Yoshida, Y., Corp, L. A., and Middleton, E. M.: First observations of global and seasonal terrestrial chlorophyll fluorescence from space, *Biogeosciences*, 8, 637–651, doi:10.5194/bg-8-637-2011, 2011.

Joiner, J., Yoshida, Y., Vasilkov, A. P., Middleton, E. M., Campbell, P. K. E., Yoshida, Y., Kuze, A., and Corp, L. A.: Filling-in of near-infrared solar lines by terrestrial fluorescence and other geophysical effects: simulations and space-based observations from SCIAMACHY and GOSAT, *Atmos. Meas. Tech.*, 5, 809–829, doi:10.5194/amt-5-809-2012, 2012.

25 Joiner, J., Guanter, L., Lindstrot, R., Voigt, M., Vasilkov, A. P., Middleton, E. M., Huemrich, K. F., Yoshida, Y., and Frankenberg, C.: Global monitoring of terrestrial chlorophyll fluorescence from moderate-spectral-resolution near-infrared satellite measurements: methodology, simulations, and application to GOME-2, *Atmos. Meas. Tech.*, 6, 2803–2823, doi:10.5194/amt-6-2803-2013, 2013.

30 Kulawik, S. S., Jones, D. B. A., Nassar, R., Irion, F. W., Worden, J. R., Bowman, K. W., Machida, T., Matsueda, H., Sawa, Y., Biraud, S. C., Fischer, M. L., and Jacobson, A. R.:

Mapping of satellite Earth observations using moving window block kriging

J. M. Tadić et al.

Title Page

Abstract

Introduction

Conclusions

References

Tables

Figures



Back

Close

Full Screen / Esc

Printer-friendly Version

Interactive Discussion



Characterization of Tropospheric Emission Spectrometer (TES) CO₂ for carbon cycle science, *Atmos. Chem. Phys.*, 10, 5601–5623, doi:10.5194/acp-10-5601-2010, 2010.

Kuze, A., Suto, H., Nakajima, M., and Hamazaki, T.: Thermal and near infrared sensor for carbon observation Fourier-transform spectrometer on the Greenhouse Gases Observing Satellite for greenhouse gases monitoring, *Appl. Optics*, 48, 6716–6733, doi:10.1364/AO.48.006716, 2009.

Lee, J.-E., Frankenberg, C., van der Tol, C., Berry, J. A., Guanter, L., Boyce, C. K., Fisher, J. B., Morrow, E., Worden, J. R., Asefi, S., Badgley, G., and Saatchi, S.: Forest productivity and water stress in Amazonia: observations from GOSAT chlorophyll fluorescence, *Proc. R. Soc. B*, 280, 1762, doi:10.1098/rspb.2013.0171, 2013.

NASA Earth Science: <http://science.nasa.gov/earth-science/earth-science-data/data-processing-levels-for-eosdis-data-products/>, last access: 23 July 2014.

O'Dell, C. W., Connor, B., Bösch, H., O'Brien, D., Frankenberg, C., Castano, R., Christi, M., Eldering, D., Fisher, B., Gunson, M., McDuffie, J., Miller, C. E., Natraj, V., Oyafuso, F., Polonsky, I., Smyth, M., Taylor, T., Toon, G. C., Wennberg, P. O., and Wunch, D.: The ACOS CO₂ retrieval algorithm – Part 1: Description and validation against synthetic observations, *Atmos. Meas. Tech.*, 5, 99–121, doi:10.5194/amt-5-99-2012, 2012.

Parazoo, N. C., Bowman, K., Frankenberg, C., Lee, J. E., Fisher, J. B., Worden, J., Jones, D. B. A., Berry, J., Collatz, G. J., Baker, I. T., Jung, M., Liu, J., and Osterman, G.: Interpreting seasonal changes in the carbon balance of southern Amazonia using measurements of XCO₂ and chlorophyll fluorescence from GOSAT, *Geophys. Res. Lett.*, 40, 2829–2833, doi:10.1002/grl.50452, 2013.

Takagi, H., Houweling, S., Andres, R. J., Belikov, D., Bril, A., Boesch, H., Butz, A., Guerlet, S., Hasekamp, O., Maksyutov, S., Morino, I., Oda, T., O'Dell, C. W., Oshchepkov, S., Parker, R., Saito, M., Uchino, O., Yokota, T., Yoshida, Y., and Valsala, V.: Influence of differences in current GOSAT XCO₂ retrievals on surface flux estimation, *Geophys. Res. Lett.*, 41, 2598–2605, doi:10.1002/2013GL059174, 2014.

Van Tooren, C. F. and Haas, T. C.: A site investigation strategy using moving window kriging and automated semivariogram modelling, in: *Contaminated Soil '93*, Kluwer Academic Press, Dordrecht, 609–622, 1993.

Walter, C., McBratney, A. B., Douaoui, A., and Minasny, B.: Spatial prediction of topsoil salinity in the Chelif Valley, Algeria, using local ordinary kriging with local variograms vs. whole-area variogram, *Aust. J. Soil Res.*, 39, 259–272, 2001.

Webster, R.: Geostatistics for engineers and earth scientists, Eur. J. Soil Sci., 51, 541–549, doi:10.1046/j.1365-2389.2000.00334-9.x, 2000.

Discussion Paper | Discussion Paper | Discussion Paper | Discussion Paper | Discussion Paper

GMDD

7, 5381–5405, 2014

Mapping of satellite Earth observations using moving window block kriging

J. M. Tadić et al.

Title Page

Abstract

Introduction

Conclusions

References

Tables

Figures



Back

Close

Full Screen / Esc

Printer-friendly Version

Interactive Discussion



Mapping of satellite Earth observations using moving window block kriging

J. M. Tadić et al.

Title Page

Abstract

Introduction

Conclusions

References

Tables

Figures



Back

Close

Full Screen / Esc

Printer-friendly Version

Interactive Discussion

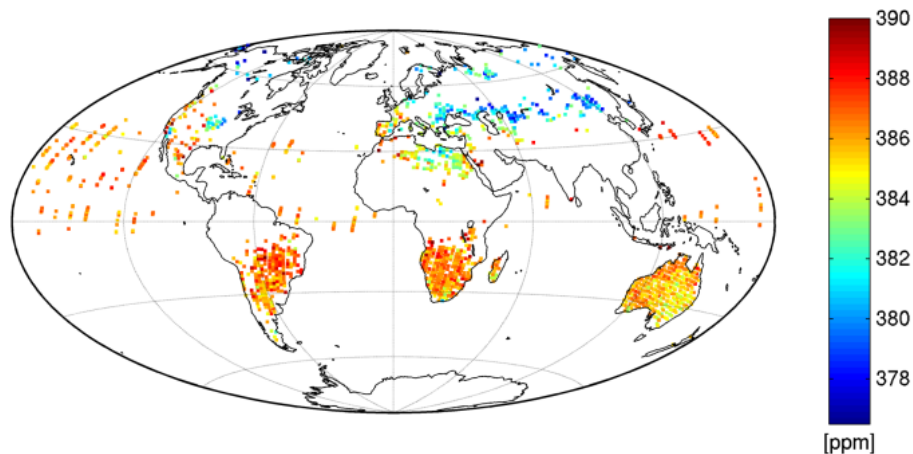


Figure 1. ACOS v3.4 release 3 XCO₂ Level 2 data (“Observations”) for 2–7 August 2009.

Mapping of satellite
Earth observations
using moving
window block kriging

J. M. Tadić et al.

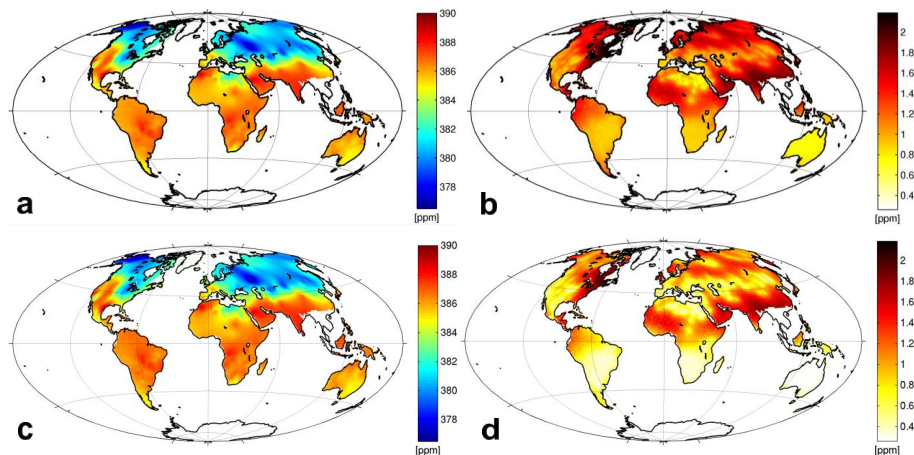


Figure 2. XCO₂ Level 3 maps (a, c) and associated uncertainties (b, d) based on ACOS 3.4 release-3 retrievals (“Estimates”) for 2–7 August 2009 at (a, b) native resolution and (c, d) 1° × 1° resolution, obtained using the proposed mapping approach.

[Title Page](#)[Abstract](#)[Introduction](#)[Conclusions](#)[References](#)[Tables](#)[Figures](#)[⏪](#)[⏩](#)[◀](#)[▶](#)[Back](#)[Close](#)[Full Screen / Esc](#)[Printer-friendly Version](#)[Interactive Discussion](#)

Mapping of satellite Earth observations using moving window block kriging

J. M. Tadić et al.

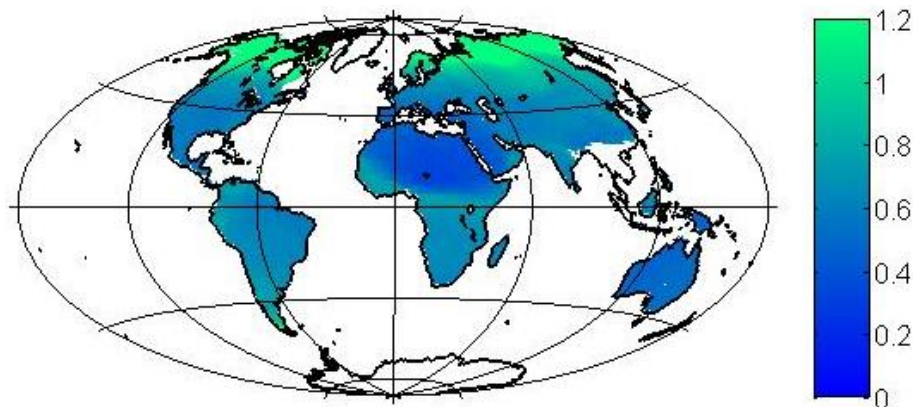


Figure 3. Reduction in estimation uncertainties between the native estimation resolution and the $1^\circ \times 1^\circ$ estimation resolution for XCO₂ Level 3 maps based on ACOS 3.4 release-3 retrievals for 2–7 August 2009.

[Title Page](#)[Abstract](#)[Introduction](#)[Conclusions](#)[References](#)[Tables](#)[Figures](#)[◀](#)[▶](#)[◀](#)[▶](#)[Back](#)[Close](#)[Full Screen / Esc](#)[Printer-friendly Version](#)[Interactive Discussion](#)

Mapping of satellite Earth observations using moving window block kriging

J. M. Tadić et al.

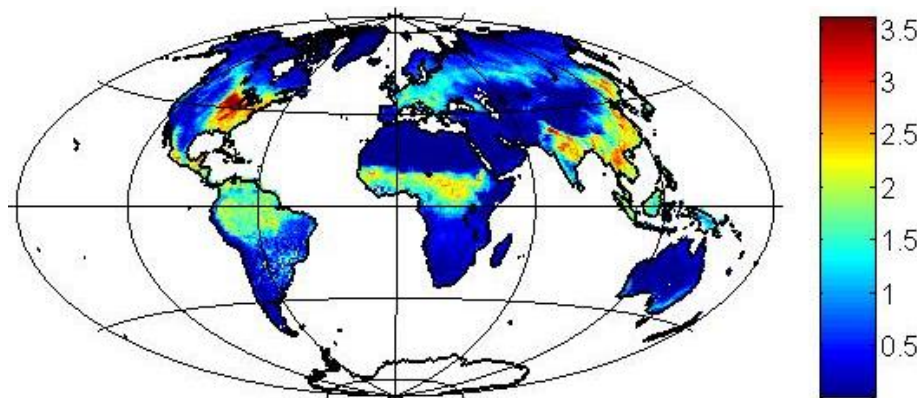


Figure 4. Monthly-averaged binned map of GOME-2 SIF data for 1–31 August 2009 ($\text{mW m}^2 \text{sr}^{-1} \text{nm}^{-1}$).

[Title Page](#)[Abstract](#)[Introduction](#)[Conclusions](#)[References](#)[Tables](#)[Figures](#)[⏪](#)[⏩](#)[◀](#)[▶](#)[Back](#)[Close](#)[Full Screen / Esc](#)[Printer-friendly Version](#)[Interactive Discussion](#)

Mapping of satellite Earth observations using moving window block kriging

J. M. Tadić et al.

Title Page

Abstract

Introduction

Conclusions

References

Tables

Figures

◀

▶

◀

▶

Back

Close

Full Screen / Esc

Printer-friendly Version

Interactive Discussion

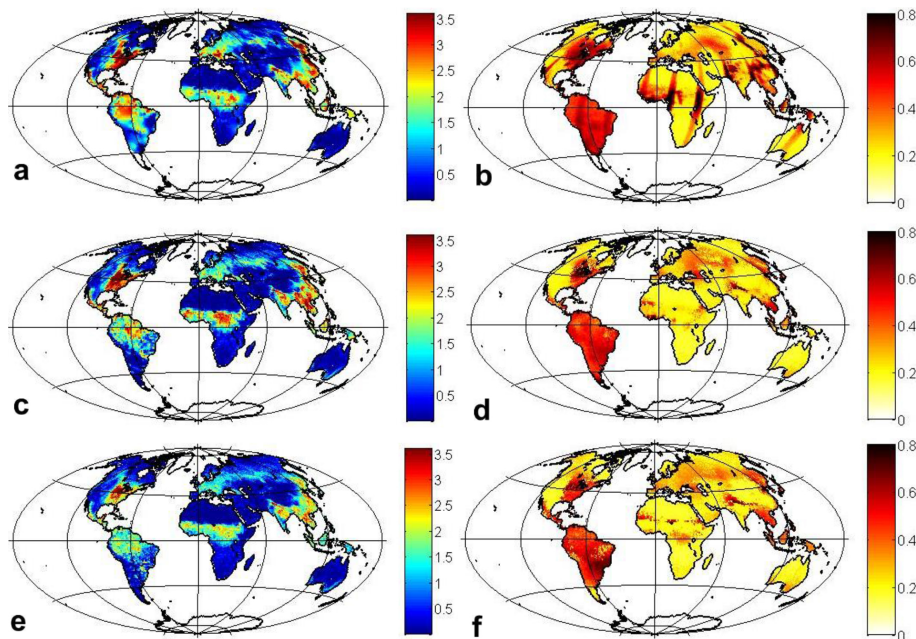


Figure 5. Maps of global SIF ($\text{mW m}^2 \text{sr}^{-1} \text{nm}^{-1}$) (**a, c, e**) and associated estimation uncertainties expressed as standard deviations (**b, d, f**), for 1 August 2009 (**a, b**), 2–7 August 2009 (**c, d**) and 1–31 August 2009 (**e, f**) obtained using GOME-2 observations (**a**) and the presented mapping approach at $1^\circ \times 1^\circ$ spatial resolution.